First-Principles Calculations of AlN Nanowires and Nanotubes: Atomic Structures, Energetics, and Surface States

Mingwen Zhao,*,† Yueyuan Xia,† Xiangdong Liu,† Zhenyu Tan,‡ Boda Huang,§ Chen Song,† and Liangmo Mei†

School of Physics and Microelectronics, School of Electric Engineering, and School of Information Science and Engineering, Shandong University, Jinan 250100, China

Received: November 21, 2005; In Final Form: March 4, 2006

We explore the atomic and electronic structures of single-crystalline aluminum nitride nanowires (AlNNWs) and thick-walled aluminum nitride nanotubes (AlNNTs) with the diameters ranging from 0.7 to 2.2 nm by using first-principles calculations and molecular dynamics simulations based on density functional theory (DFT). We find that the preferable lateral facets of AlNNWs and thick-walled AlNNTs are $\{10\bar{1}0\}$ surfaces, giving rise to hexagonal cross sections. Quite different from the cylindrical network of hexagons revealed in single-walled AlNNTs, the wall of thick-walled AlNNTs displays a wurtzite structure. The strain energies per atom in AlNNWs are proportional to the inverse of the wire diameter, whereas those in thick-walled AlNNTs are independent of tube diameter but proportional to the inverse of the wall thickness. Thick-walled AlNNTs are energetically comparable to AlNNWs of similar diameter, and both of them are energetically more favorable than single-walled AlNNTs. Both AlNNWs and AlNNTs are wide band gap semiconductors accompanied with surface states located in the band gap of bulk wurtzite AlN.

Introduction

One-dimensional III−V semiconductor nanostructures are attracting great interest for their promising high impact in optoelectronics applications, such as optoelectronic devices in the UV and visible region. Aluminum nitride nanowires (AlNNWs) and nanotubes (AlNNTs) appear to be promising materials, due to their large band gap of ∼6.2 eV[1] and low electron affinity.[2] Randomly oriented AlNNWs[3,4] and AlNNTs,[5] as well as aligned AlNNWs,[6,7] have been fabricated typically by the reaction of Al alloy in an NH_3/N_2 atmosphere. These as-synthesized AlNNWs and AlNNTs are of single-crystalline wurtzite structure with the growth direction of [0001]. So far little is known about their lateral facets. The diameters of these wires are in the range of 10 to ∼100 nm,[7] while AlNNTs are typically 30 to ∼80 nm in outer diameter with the wall thickness of several nanometers.[4] The adsorption edge of AlNNWs is blue-shifted by ∼0.27 eV from the bulk edge as revealed by transmission spectra,[7] which has been attributed to the quantum size effect in the radial direction.[8]

Theoretical efforts, on the other hand, have been devoted to the atomic and electronic structures of single-walled AlNNTs by analogy with single-walled carbon nanotubes.[9,10] However, the cylindrical network of hexagons in single-walled AlNNTs is quite different from the as-synthesized AlNNTs which always have thick walls with wurtzite structure. So far, the realization of single-walled AlNNTs remains a great experimental challenge because of their high strain energy with respect to that of the bulk materials.[9] Very recently, based on first-principles calculations, a new configuration of an individual faceted AlNNT which has lower strain energy than that of single-walled AlNNTs was reported.[11] This may be a promising candidate for modeling the as-synthesized AlNNTs due to its highly energetic advantage. However, up to now, the atomic configurations of thick-walled AlNNTs with wide-ranged sizes and the variation of the strain energy with diameter have not been reported. The studies of these interesting issues are not only very helpful for determining the morphologies of AlNNWs and AlNNTs at the atomic scale but also valuable for shedding light on the growth mechanisms of these promising nanomaterials.

Moreover, motivated by the fascinating electronic properties of carbon nanotubes, considerable effort has been contributed to explore the electronic structures of other tubular nanomaterials, such as AlN,[9] BN,[12] GaN,[13] and SiC,[14] for their promising application in building nanodevices. Mainly due to the localization of electronic states in these materials, few of them have the diverse electronic properties from metallic to semiconducting, as those of carbon nanotubes. Very recently, Rurali and co-workers, based on their first-principles calculations, predicted that the reconstruction on the lateral facets of Si[15] and SiC[16] nanowires could metalize these nanowires by the formation of surface states, although their bulk materials are semiconductor. This indicates that the surface states may play a crucial role in the electronic properties of one-dimensional nanomaterials. However, the study of effects of surface states on AlNNWs and AlNNTs is still missing.

To fill this gap of knowledge, we explored in this contribution the atomic configurations, strain energies, and electronic structures of AlNNWs and AlNNTs with the diameter ranging from 0.7 to 2.2 nm, by using first-principles calculations based on density functional theory (DFT). A possible growth mechanism of AlN nanotubes was also discussed on the basis of these calculations.

* Corresponding author. E-mail: zmw@sdu.edu.cn.
† School of Physics and Microelectronics.
‡ School of Electric Engineering.
§ School of Information Science and Engineering.

10.1021/jp056755f CCC: $33.50
Published on Web 04/08/2006

Computational Methods

We performed first-principles calculations by using SIESTA.[17−19] This code is based on the standard Kohn−Sham self-consistent DFT and adopts a flexible linear combination of numerical atomic orbital basis sets for valence electrons and norm-conserving nonlocal pseudopotentials for the atomic core. The Perdew, Burke, and Ernzerhof (PBE) form generalized gradient approximation (GGA) corrections were employed for the exchange-correlation potential.[20] The atomic orbital basis set employed throughout was a double-ζ plus polarization functions (DZP). The numerical integrals were preformed on a real space grid with an equivalent cutoff of 100 Ry. Periodic boundary condition along the axis was employed for nanowires and nanotubes, while a vacuum region up to 10 Å was set to decouple the interaction between adjacent wires and tubes. The size of the supercells adopted in these calculations was minimized (primitive cell) which contain up to 192 atoms. Brillouin zones were sampled by a set of k-points grid ($1 \times 1 \times 8$) for nanowires and nanotubes and ($4 \times 4 \times 4$) for bulk AlN (wurtzite) according to the Monkhorst−Pack approximation.[21] All the atomic coordinates along with the supercells were fully relaxed with a conjugate gradient (CG) algorithm, until each component of the stress tensor was below 0.5 GPa and the maximum atomic forces were <0.04 eV/Å. This computational scheme is convergent and reproduces well the equilibrium lattice parameters of wurtzite AlN with $a = 3.176$ Å and $c/a = 1.599$ which are very close to the experimental results, $a = 3.114$ Å and $c/a = 1.601$ (Joint Committee on Powder Diffraction Standards card no. 08-0262). The strain energy (E_{Strain}) was calculated by the difference between the total energy per atom of AlN nanowires or nanotubes and that of wurtzite AlN. The surface energy was evaluated under the supposition that the strain of AlN nanowires and nanotubes mainly arises from the surface (exterior and interior) atoms and distributes uniformly on these surfaces.

Results and Discussion

The axial orientation of the as-synthesized AlNNWs and AlNNTs is always in the [0001] direction accompanied with hexagonal cross sections,[4] whereas no experimental result for determining the lateral facet orientations of AlNNWs and AlNNTs is available so far. By analogy with single-crystalline GaN nanotubes,[22,23] we tried to model the lateral facets of AlNNWs and AlNNTs with $\{10\bar{1}0\}$ and $\{11\bar{2}0\}$ surfaces, respectively. We first adopted a slab supercell along with periodical boundary condition to determine the surface energies of infinite two-dimensional AlN $(10\bar{1}0)$ and $(11\bar{2}0)$ surfaces and found that they are 136 meV/Å^2 and 143 meV/Å^2, respectively. We attribute the energetic advantage of the AlN $(10\bar{1}0)$ surface to the lower density of dangling bonds which is 0.12/Å^2 as compared to 0.14/Å^2 of the AlN $(11\bar{2}0)$ surface. A similar result has also been reported for GaN nanowires which are 118 meV/Å^2 and 123 meV/Å^2 for $(10\bar{1}0)$ and $(11\bar{2}0)$ surfaces, respectively.[24]

We then calculated the strain energies in AlNNWs with different lateral facets. Figure 1, parts b and c, gives the equilibrium configurations of two AlNNWs with similar diameters, 16 Å and 15.6 Å, but different lateral facets, $\{10\bar{1}0\}$ and $\{11\bar{2}0\}$, respectively. The AlNNW with $\{10\bar{1}0\}$ lateral facets is found to be energetically more favorable than the $\{11\bar{2}0\}$-faceted AlNNW by about 94 meV/atom from our calculations. The surface energies of these nanowires are 153 meV/Å^2 and 156 meV/Å^2, respectively, slightly higher than that obtained from an infinite two-dimensional surface. We attribute these differences to the atoms in the corners of the hexagonal cross section of the nanowires whose coordinate environment is quite different from that of the atoms on infinite two-dimensional surfaces, and thus the Al−N bonds associated to these atoms are shortened to about 1.82 Å as compared to those of other atoms (see Figure 1b). The above results clearly indicate that the preferable lateral facets of AlNNWs are $\{10\bar{1}0\}$ surfaces rather than $\{11\bar{2}0\}$ surfaces. We thus focus on AlNNWs and AlNNTs with $\{10\bar{1}0\}$ facets in the present work. But it should be noticed that $\{10\bar{1}0\}$ facets could form AlNNWs with hexagonal and distorted hexagonal cross sections, as viewed along the circumference formed by the outermost hexagons on the cross sections, as shown in the insets of Figure 2. However, the variations of the strain energies of the AlNNWs and AlNNTs with these cross sections as a function of diameter are similar (see Figure 2).

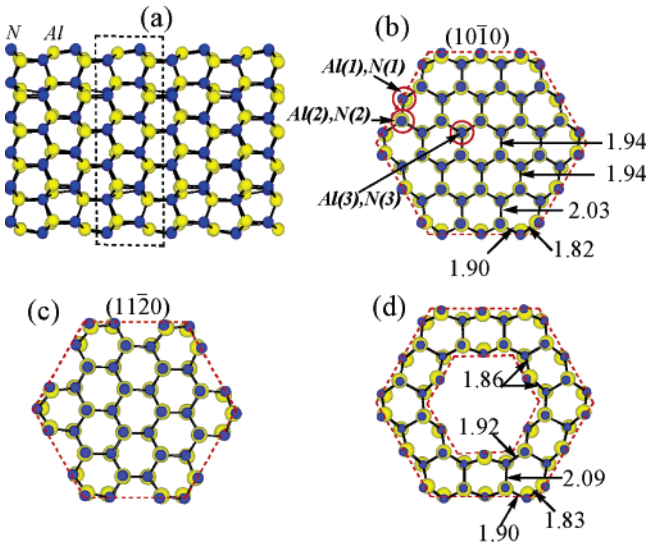

Figure 1. Equilibrium configurations of an AlNNW and an AlNNT: (a) side view and (b) top view of an AlNNW with $\{10\bar{1}0\}$ lateral facets; (c) top view of an AlNNW with $\{11\bar{2}0\}$ facets; (d) top view of a double-walled AlNNT with the lateral facets of $\{10\bar{1}0\}$.

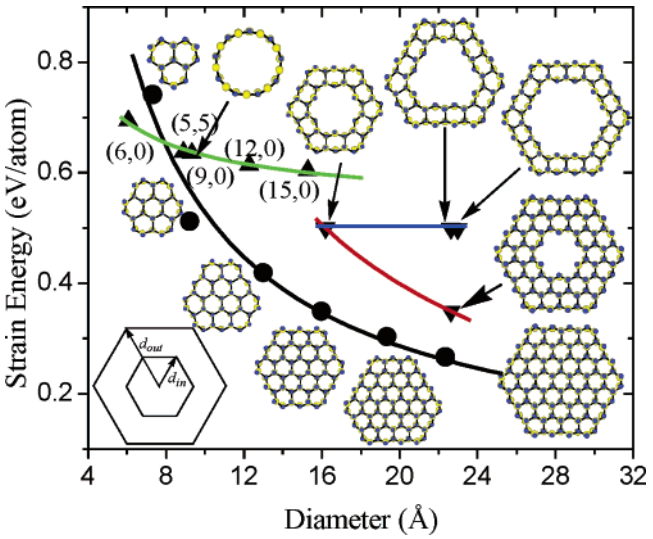

Figure 2. Strain energies of AlNNWs and AlNNTs relative to bulk wurtzite AlN as a function of diameter. The strain energies of AlNNWs are represented by the solid circles, while the black line is the fitting curve by using the expression $E_{Strain} = C/d$, with $C = 4.828$ eV Å. The strain energies of multiwalled AlNNTs and single-walled AlNNTs are denoted by the down triangles and up triangles, respectively.

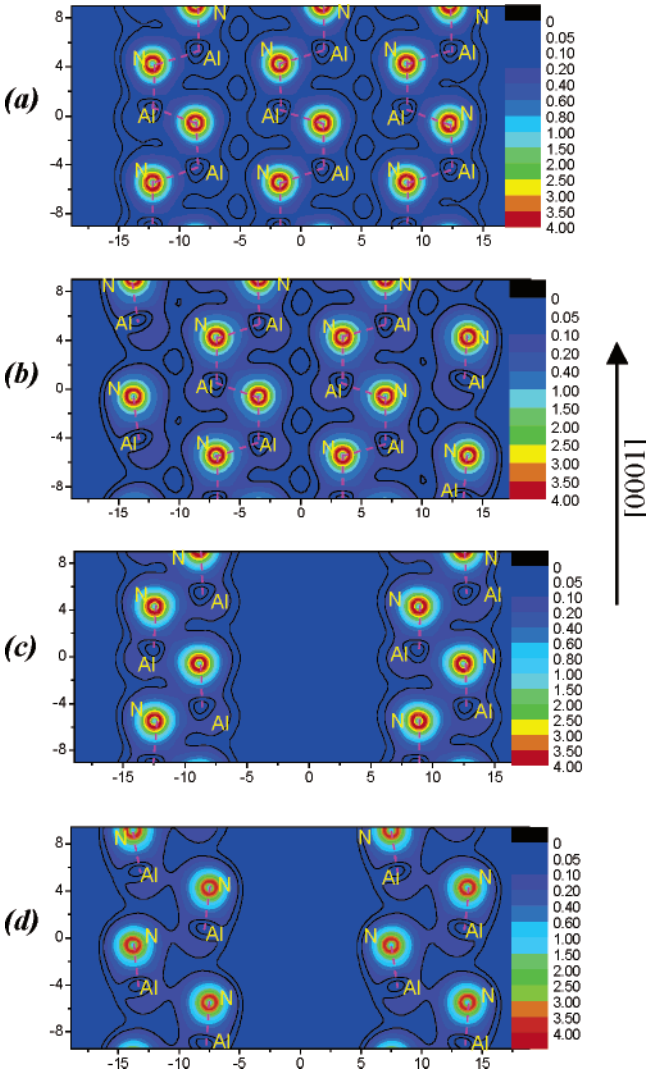

Figure 3. Valence electron density distribution on $(11\bar{2}0)$ faces sampled at the two different locations of the AlNNW shown in Figure 1b and AlNNT shown in Figure 1d: (a and b) for the AlNNW; (c and d) for the AlNNT. Dashed lines indicate the ionic Al−N bonds.

Figure 1b gives the top view of equilibrium configuration of an AlNNW with the diameter of 16 Å. In the core of this wire, the bond length of the Al−N bond is about 1.94 Å and the bond angle is ∼109° which are very close to those in wurtzite AlN. A slight distortion occurs near the surfaces, which shortens the Al−N bond lengths on the surfaces to 1.82 ∼1.91 Å, whereas it elongates the Al−N bonds between the surface atoms and the core atoms to ∼2.03 Å (see Figure 1b). Al atoms move toward the tube axis while N atoms move in the opposite direction on the surfaces, resulting in a relative radial displacement, 0.24 Å, between Al and N atoms. Therefore, the centers of positive charges and negative charges no more coincide in the radial direction (see Figure 3b), resulting in surface dipoles which maybe responsible for the electronic and optoelectronic properties of AlNNWs and AlNNTs, such as field-emission.[24]

As well, we modeled thick-walled AlNNTs with both the outer and inner facets with $\{10\bar{1}0\}$ surfaces (as shown in Figure 1d and the insets of Figure 2). These AlNNTs have walls containing two and three atomic layers, and thus are named as double- and triple-walled AlNNTs, by analogy with carbon nanotubes. The equilibrium configuration of a double-walled AlNNT with the diameter of 16 Å and the wall thickness of 4.17 Å is shown in Figure 1d. It is clear that the morphologies of these thick-walled tubes are quite different from that of single-walled AlNNTs which always have rounded cross sections.[9] Moreover, the wall of these thick-walled AlNNTs clearly displays the character of the wurtzite structure, despite slight distortion on the lateral facets, unlike the layered structure of multiwalled carbon nanotubes. Because of the surface relaxation in double-walled AlNNTs, the Al−N bonds on the outer and the inner surfaces are compressed to 1.83 ∼1.93 Å, whereas the bonds between the inner and the outer surfaces are elongated to 2.08 ∼2.14 Å, as compared to 1.94 Å of wurtzite AlN. On the outer facets, Al atoms move toward the tube axis and N atoms move in opposite direction, whereas the Al and N atoms on the inner facets are displayed reversedly (as shown in Figure 1d and Figure 3d), giving rise to a relatively radial displacement of 0.24 Å for the surface Al and N atoms. Surface dipoles along the radial direction are induced on both outer and inner facets (see Figure 3d). Similar distortion has also been revealed in triple-walled AlNNTs. These surface dipoles may also be responsible for the growth mechanisms of AlNNTs.

The strain energies, E_{Strain}, of AlNNWs and AlNNTs, relative to that of wurtzite AlN, as a function of diameter d are plotted in Figure 2. The diameter d was determined by the average of radial distance between the central axis and the outermost atoms. The black line is the fitting curve for AlNNWs by using the expression of $E_{\text{Strain}} = C/d$ with $C = 4.828$ eV Å. For thick-walled AlNNTs, things are quite different, however. The strain energies of double-walled AlNNTs with three different diameters keep constant, ∼0.50 eV/atom, as represented by the down triangles connected by the blue line as shown in Figure 2. The strain energy of a triple-walled AlNNT is greatly reduced to 0.35 eV/atom, which is comparable to that of 0.27 eV/atom of an AlNNW with the same diameter. The variation of the strain energies with diameter of thick-walled AlNNTs is completely different from that of single-walled AlNNTs,[9] which decreases monotonically with the increasing tube diameter and saturates at the value corresponding to the AlN graphitic-like sheet (as shown by the up triangles in Figure 2).

The strain energy variation of these AlNNWs and thick-walled AlNNTs can be easily understood since the strain energy mainly arises from the curvature of the external and internal surfaces and the local structural distortion of the atoms on the surfaces. The structural distortion mainly occurs near the surfaces, whereas the deviation of bond lengths and bond angles in the core region from those of a perfect wurtzite AlN crystal is quite small, as revealed in our calculations (see Figure 1b). The strain energy of thick-walled AlNNTs, E_{Strain}, can therefore be approximately evaluated by the expression

$$E_{\text{Strain}} = \frac{8E_{\text{Suf}}}{\sqrt{3}n(d_{\text{out}} - d_{\text{in}})}$$

where E_{Suf} is the surface energy of the $(10\bar{1}0)$ surface, n is the atomic density, and d_{out} and d_{in} are the outer and inner diameters of thick-walled AlNNTs (see the inset of Figure 2). Obviously, according to this expression, the strain energy of thick-walled AlNNTs is proportional to the inverse of wall thinness and independent of tube diameter. We evaluated the E_{Strain} of double- and triple-walled AlN nanotubes that are 0.53 and 0.35 eV/atom, respectively, by using this expression with $E_{\text{Suf}} = 136$ meV/Å^2, $n = 0.14$/Å^3 for the double-walled AlNNT and 0.12/Å^3 for the triple-walled AlNNT. They are in good agreement with 0.50 and 0.35 eV/atom for double-walled AlNNT and triple-walled AlNNT, respectively, obtained by direct first-

principles calculations. This expression is also valid for describing AlNNTs with $d_{in} = 0$ and reproduces well their strain energies.

We also found that when the thickness of the wall of AlNNT is reduced to a single atomic layer, the hexagonal cross section is unstable and transforms to a round cross section after relaxation, forming a zigzag single-walled AlNNT. For example, the double-walled AlNNT corresponding to Figure 1d can be disassembled into two individual (9, 0) and (15, 0) single-walled AlNNTs, respectively. But the strain energies increase to 0.635 eV/atom for (9, 0) and 0.605 eV/atom for (15, 0) tubes (represented by the up triangles in Figure 2) as compared to 0.50 eV/atom of the double-walled AlNNTs. The unfavorable energetics of the single-walled AlNNTs in comparison with those of thick-walled AlNNTs and AlNNWs clearly confirms the difficulties in fabricating single-walled AlNNTs. More interestingly, when the configuration containing coaxial (9, 0) and (15, 0) single-walled AlNNTs with rounded cross sections, similar to double-walled carbon nanotubes, was heated at 1000 K for 2 ps by using Nose dynamics, a distorted hexagonal cross section will be obtained by the formation of ionic Al−N bonds between the inner and the outer surfaces. Although, we cannot obtain the ground state configuration corresponding to Figure 1d starting from the coaxial (9, 0) and (15, 0) AlNNTs from the present simulations, partly due to the limitation of available CPU time scale, the tendency of transition to the configuration is very obvious. The ionic binding between the inner and the outer surfaces in the double-walled AlNNTs (as seen in Figure 3c) are much stronger than that of the van der Waals interactions which dominate the coupling between the inner and the outer layers in double-walled carbon nanotubes. This further confirms the great challenge of realizing single-walled AlNNTs.

To test the thermal stability of AlNNWs and AlNNTs, we heated them at the temperatures of 300, 500, and 800 K, respectively, for 2 ps by using Nose dynamics. We found that the AlNNW corresponding to the configuration as shown in Figure 1b can stably exist at the temperature as high as 800 K. However, the structural disorder of double-walled AlNNT as shown in Figure 1d caused by atomic thermal motion becomes significant with the average root mean square deviations (rmsd) as high as 0.9 Å, as the temperature is higher than 500 K, clearly indicating that it starts to melt. This is related to the higher strain energy involved in AlNNTs as compared to that in AlNNWs.

Single-walled AlNNTs, as metastable states, may only exist under special conditions due to their high strain energies. If a single-walled AlNNT was formed, the growth of the tube wall along radial direction would not stop immediately. It would adsorb the incoming AlN species in the environment and form thick-walled AlNNTs with hexagonal cross sections in order to release the strain energy. The surface dipoles on the lateral facets of AlNNTs facilitate the adsorption of polar AlN species and thus keep the growth of tube wall continued along the radial direction. This may be the reason the as-synthesized AlN nanotubes always have a thick wall.[3−7] Controlling the surface dipoles may be helpful for synthesizing ultrathin AlNNTs or even single-walled AlNNTs.

Finally, we calculated the band structures of an AlNNW and a thick-walled AlNNT corresponding to the configurations shown in Figure 1, parts b and d, and display them in Figure 4, parts b and c, respectively. The band structures of bulk AlN (wurtzite) and a single-walled (9, 0) AlNNT are also presented in Figure 4, parts a and d, respectively, for comparison. Wurtzite AlN has a direct band gap of about 3.86 eV at the Γ point along

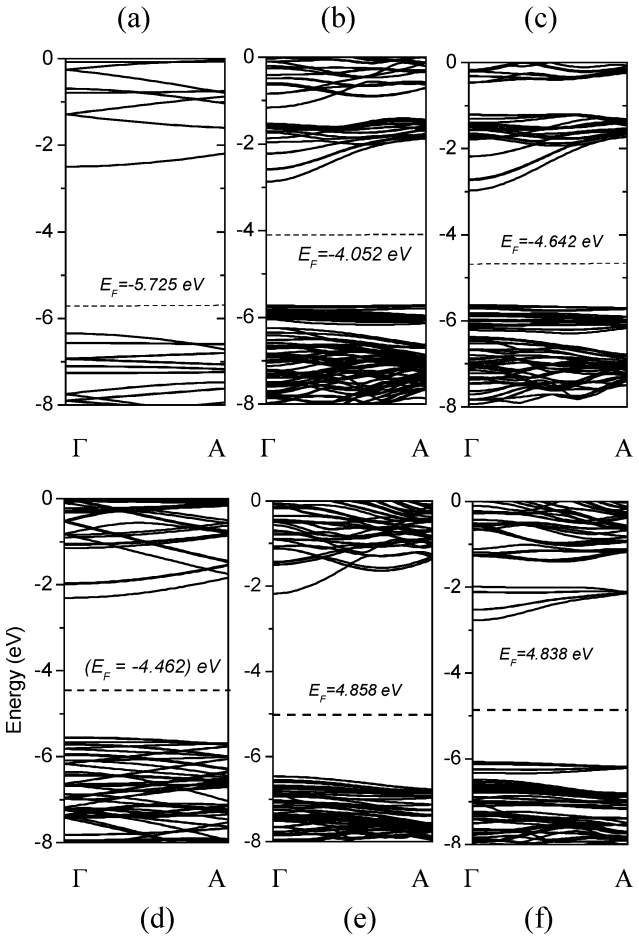

Figure 4. Band structures along the direction from Γ(0, 0, 0) π/a to A(0, 0, 0.5) $2\pi/a$ of (a) bulk AlN (wurtzite); (b) AlNNW corresponding to the configuration of Figure 1b; (c) AlNNT with the configuration of Figure 1d; and (d) single-walled (9, 0) AlNNT. The dashed lines represent the Fermi levels (E_F) which were directly obtained from Fermi−Dirac distribution at room temperature. The E_F of bulk AlN (wurtzite) was calculated in the whole Brillouin zone with the *k*-points mesh 4 × 4 × 4, while only the band lines along the Γ−A direction are presented in this figure. So the E_F is not closer to the midgap in (a).

the Γ(0, 0, 0) $2\pi/a$−A(0, 0, 0.5) $2\pi/a$ direction in reciprocal spaces. This value is much smaller than that of experimental result, 6.2 eV, mainly due to the well-known shortcoming of DFT in describing excited states. The band gaps obtained from the present calculations are therefore incomparable to the experimental results. However, despite the underestimation of the gap width, DFT is known to reproduce extremely well the occupied states and the dispersion of the bands. The band structures of the AlNNW and thick-walled AlNNT clearly indicate that some bands appear in the band gap of bulk AlN (wurtzite). These bands are very smooth and thus highly localized in real space. Further analysis on project density of states (PDOS) shows that they mainly arise from the states of the atoms on the facets (as shown in Figure 5), clearly indicating that there are surface states. This is quite different from the result that no surface state exists in the gap on a clean GaN $(10\bar{1}0)$ surface.[18] Occupied surface bands arise from the states of N atoms, while unoccupied surface bands arise from the states of Al atoms, respectively (see Figure 5). This is consistent with the asymmetry of charge distribution on the surfaces where the valence electron density is strongly accumulated around the N atoms because of their strong 2p potentials (as shown in Figure 3). The band structures of single-walled (9, 0) AlNNT, on the

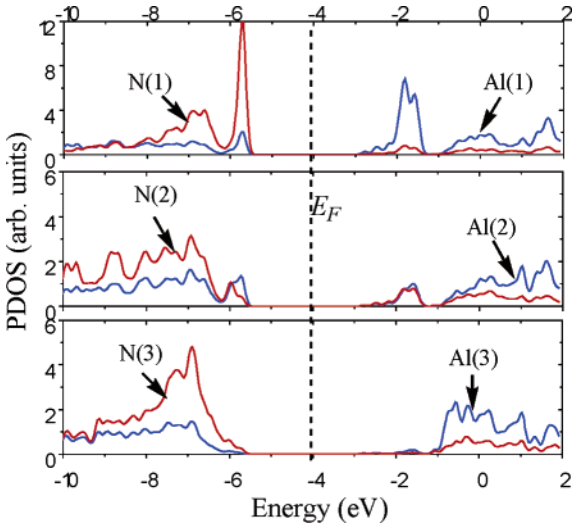

Figure 5. Electron density of states (DOS) projected onto different atoms labeled in Figure 1b. The dashed line is the Fermi level.

other hand, bear no resemblance to those of bulk AlN, because their configurations are completely different. The width of the occupied surface bands of the AlNNW is about 0.45 eV with its frontier state 0.52 eV above the top of the valence band of wurtzite AlN (Figure 4b). For the thick-walled AlNNT, the width of occupied surface bands is extended to 0.66 eV and the frontier surface state is 0.74 eV above the top of the valence band of wurtzite AlN (Figure 4c), due to the contribution from the atoms on the inner facets. These surface states have narrowed the band gap and thus should definitely be responsible for the electronic properties of AlNNWs and AlNNTs. The effect of surface states is contrary to the quantum size effect which opens the band gap up. The experimental results of AlNNWs and thick-walled AlNNTs with clean facets, such as the blue shift of the adsorption edge, should reflect the competition of these two effects. Unfortunately, due to the limitation of DFT itself, the gap-opening effect cannot be reproduced by the present calculations. Moreover, it should be noticed that when the lateral facets of AlNNWs and AlNNTs are passivated by oxide layers, the surface states might be quite different. As a test, we calculated the band structures of an AlNNW and an AlNNW corresponding to the configurations as shown in Figure 1, parts b and d, with each atom on their exterior facets being hydrogenated. The surface bands located in the band gap of the clean AlNNW disappear in the hydrogen-passivated AlNNW, as shown in Figure 4e. However, the surface bands remain in the band gap of the hydrogen-passivated AlNNT, as shown in Figure 4f, which is related to the unsaturated bonds at the interior facets. This also confirms that the flat bands located in band gaps of clean AlNNW and AlNNT are surface bands.

Conclusions

In summary, our first-principles calculations show that the energetically favorable lateral facets of AlNNWs and thick-walled AlNNTs are $\{10\bar{1}0\}$ surfaces accompanied with formation of hexagonal cross sections. The strain energies of AlNNWs are proportional to the inverse of the wire diameter, whereas those of thick-walled AlNNTs are independent of tube diameter but proportional to the inverse of the wall thickness. The ab initio molecular dynamics simulations show that a coaxial (9, 0) and (15, 0) single-walled AlNNTs complex has a definite trend of transferring to a double-walled AlNNT at an annealing temperature, 1000 K. Both AlNNWs and AlNNTs are energetically more favorable than single-walled AlNNTs with rounded cross sections. Both AlNNWs and AlNNTs are wide band gap semiconductors with surface states located in the band gap of bulk AlN.

Acknowledgment. This work is supported by the National Natural Science Foundation of China under Grant Nos. 50402017, 10374059, and 90203013 and the National Basic Research 973 Program of China (Grant No. 2005CB623602).

References and Notes

(1) Vurgaftman, I.; Meyer, J. R.; Ram-Mohan, L. R. *J. Appl. Phys.* **2001**, *89*, 5815.
(2) Grabowski, S. P.; Schneider, M.; Nienhaus, H.; Monch, W.; Dimitrov, R.; Ambacher, O.; Stutzmann, M. *Appl. Phys. Lett.* **2001**, *78*, 2503.
(3) Xu, Q.; Hu, Z.; Wang, X.; Lu, Y.; Huo, K.; Deng, S.; Xu, N.; Chen, B.; Zhang, R.; Chen, Y. *J. Mater. Chem.* **2003**, *13*, 2024.
(4) Xu, Q.; Hu, Z.; Wang, X.; Lu, Y.; Chen, X.; Xu, H.; Chen, Y. *J. Am. Chem. Soc.* **2003**, *125*, 10176.
(5) Duan, J. H.; Yang, S. G.; Liu, H. W.; Gong, J. F.; Guang, H. B.; Zhao, X. N.; Zhang, R.; Du, Y. W. *J. Phys. Chem. B* **2005**, *109*, 3701.
(6) Xu, Q.; Hu, Z.; Wang, X.; Hu, Y.; Tian, Y.; Chen, Y. *Diamond Relat. Mater.* **2004**, *13*, 38.
(7) Zhao, Q.; Zhang, H.; Xu, X.; Wang, Z.; Xu, J.; Yu, D.; Li, G.; Su, F. *Appl. Phys. Lett.* **2005**, *86*, 193101.
(8) Brus, L. E. *J. Chem. Phys.* **1984**, *80*, 4403.
(9) Zhao, M. W.; Xia, Y. Y.; Zhang, D. J.; Mei, L. M. *Phys. Rev. B* **2003**, *68*, 235415.
(10) Zhao, M. W.; Xia, Y. Y.; Tan, Z. Y.; Liu, X. D.; Li, F.; Huang, B. D.; Ji, Y. J.; Mei, L. M. *Chem. Phys. Lett.* **2004**, *389*, 160.
(11) Chen, X.; Ma, J.; Hu, Z.; Wu, Q.; Chen, Y. *J. Am. Chem. Soc.* **2005**, *127*, 7982.
(12) Rubio, A.; Corkill, J. L.; Cohen, M. L. *Phys. Rev. B* **1994**, *49*, 5081.
(13) Lee, S. M.; Lee, Y. H.; Hwang, Y. G.; Elsner, J.; Porezag, D.; Frauenheim, Th. *Phys. Rev. B* **1999**, *60*, 7788.
(14) Zhao, M. W.; Xia, Y. Y.; Li, F.; Zhang, R. Q.; Lee, S. T. *Phys. Rev. B* **2005**, *71*, 085312.
(15) Rurali, R.; Lorente, N. *Phys. Rev. Lett.* **2005**, *94*, 026805.
(16) Rurali, R. *Phys. Rev. B* **2005**, *71*, 205405.
(17) Ordejón, P.; Artacho, E.; Soler, J. M. *Phys. Rev. B* **1996**, *53*, R10441.
(18) Sánchez-Portal, D.; Ordejón, P.; Artacho, E.; Soler, J. M. *Int. J. Quantum Chem.* **1997**, *65*, 453.
(19) Soler, J. M.; Artacho, E.; Gale, J. D.; García, A.; Junquera, J.; Ordejón P.; Sánchez-Portal, D. *J. Phys.: Condens. Matter* **2002**, *14*, 2745.
(20) Perdew, J. P.; Burke, K.; Ernzerhof, M. *Phys. Rev. Lett.* **1996**, *77*, 3865; **1997**, *78*, 1396.
(21) Monkhorst, H. J.; Pack, J. D. *Phys. Rev. B* **1976**, *13*, 5188.
(22) Xu, B.; Lu, A. J.; Pan, B. C.; Yu, Q. X. *Phys. Rev. B* **2005**, *71*, 125434.
(23) Goldberger, J.; He, R. R.; Zhang, Y. F.; Lee, S.; Yan, H. Q.; Choi, H.-J.; Yang, P. D. *Nature (London)* **2003**, *422*, 599.
(24) Northrup, J. E.; Neugebauer, J. *Phys. Rev. B* **1996**, *53*, R10477.
(25) Taniyasu, Y.; Kasu, M.; Makimoto, T. *Appl. Phys. Lett.* **2004**, *84*, 2115.